Radiol Phys Technol (2009) 2:175–182
DOI 10.1007/s12194-009-0062-5

Application of an artificial neural network to the computer-aided differentiation of focal liver disease in MR imaging

Xuejun Zhang · Masayuki Kanematsu · Hiroshi Fujita · Xiangrong Zhou · Takeshi Hara · Ryujiro Yokoyama · Hiroaki Hoshi

Received: 14 January 2009 / Revised: 16 April 2009 / Accepted: 19 April 2009 / Published online: 14 May 2009

Abstract The differentiation of focal liver lesions in magnetic resonance (MR) imaging is primarily based on the intensity and homogeneity of lesions with different imaging sequences. However, these imaging findings are falsely interpreted in some patients because of the complexities involved. Our aim is to establish a computer-aided diagnosis system named LiverANN for classifying the pathologies of focal liver lesions into five categories using the artificial neural network (ANN) technique. On each MR image, a region of interest (ROI) in the focal liver lesion was delineated by a radiologist. The intensity and homogeneity within the ROI were calculated automatically, producing numerical data that were analyzed by feeding them into the LiverANN as inputs. Outputs were the following five pathologic categories of hepatic disease: hepatic cyst, hepatocellular carcinoma, dysplasia in cirrhosis, cavernous hemangioma, and metastasis. Of the 320 MR images obtained from 80 patients (four images per patient) with liver lesions, our LiverANN classified 50 cases of a training set into five types of liver lesions with a training accuracy of 100% and 30 test cases with a testing accuracy of 93%. The experiment demonstrated that our LiverANN, which functions as a computer-aided differentiation tool, can provide radiologists with a second opinion during the radiologic diagnostic procedure.

Keywords MR imaging · Focal liver disease · Differentiation · Artificial neural network · Computer-aided diagnosis (CAD)

X. Zhang (✉)
Department of Electronics and Information Engineering,
School of Computer, Electronics and Information,
Guangxi University, 530004 Nanning, Guangxi,
People's Republic of China
e-mail: xjzhang@gxu.edu.cn

M. Kanematsu · R. Yokoyama · H. Hoshi
Department of Radiology,
Gifu University School of Medicine, Gifu, Japan

H. Fujita · X. Zhou · T. Hara
Division of Regeneration and Advanced Medical Sciences,
Department of Intelligent Image Information,
Graduate School of Medicine, Gifu University, Gifu, Japan

1 Introduction

Each year, more than 25 million Americans are afflicted with liver and gallbladder diseases, which take the lives of more than 25,000 Americans and rank eighth among the commonest causes of death. Hepatocellular carcinoma (HCC) is the most common primary neoplasm of the liver, accounting for approximately half a million deaths annually worldwide [1]. In addition, the liver is one of the organs most commonly associated with metastatic diseases, which arise most frequently from the primary sites located in the colon, breast, lung, pancreas, and stomach. Further, malignant tumor-mimicking conditions such as dysplasia in cirrhosis, cavernous hemangioma, or liver cyst must be accurately diagnosed and differentiated from malignancy, which may predispose to diagnostic dilemma in daily radiologic practice [2]. An early diagnosis provides the opportunity for hepatectomy, liver transplant, or other interventional treatments that may play a curative or palliative role.

Much research on liver analysis and segmentation is being conducted worldwide, using imaging modalities such as ultrasonography, magnetic resonance (MR) imaging, computed tomography (CT), and positron emission tomography (PET). The use of ultrasonography is less invasive, but the visual criteria are generally confusing and highly subjective, with a diagnostic accuracy of approximately 70% [3–6] for

radiologists. In order to assist physicians in the characterization of liver tissues, Ogawa et al. [7] developed a computer-aided diagnosis (CAD) system with ultrasonography for diffuse liver diseases that uses neural networks. Wang et al. [8] carried out a texture analysis using a co-occurrence matrix to investigate the existence of liver cirrhosis via ultrasonography. Owing to the high image quality and shorter acquisition time, CT images are suitable for the detection of liver diseases and segmentation in the virtual planning of a liver surgery. Bae et al. [9] proposed a method of extracting the liver structure from CT images based on a gray-level thresholding technique. Selle et al. [10] analyzed and visualized the hepatic vascular structures when planning liver surgery.

Despite the advances in CAD for CT, the characterization of a focal liver lesion is yet to be achieved by this method. To date, only a few CAD studies on MR images are available, particularly on the differentiation of liver disease. Tombropoulos et al. [11] used a knowledge base of MR imaging findings and a belief-network inference engine to generate probabilistic differential diagnoses for 12 types of hepatic lesions. However, inputting all of the clinical information and the information inferred by the system from segmented MR imaging is not practical in clinical use or medical training. Maclin et al. [12] have devised a plan for improving the diagnostic accuracy of the neural networks that includes MR imaging and CT data. However, follow-up on their experimental results is not currently feasible.

Because of its advantage of good spatial and contrast resolution, MR imaging is used for the detection and characterization of focal liver lesions in radiological practice. Typically, in MR imaging of the liver, radiologists interpret several MR images obtained with different pulse sequences with and without contrast enhancement to make a diagnosis. However, these imaging findings are falsely interpreted for some patients because of the complexities involved [13]. Our aim is to establish a CAD system for distinguishing the pathologies of focal liver lesions on MR images; this system is expected to assist radiologists in integrating MR imaging findings with different pulse sequences (precontrast T1-weighted, fast spin-echo (FSE) T2-weighted, and gadolinium-enhanced MR images) and to raise the diagnostic accuracy of imaging when performed by even inexperienced radiologists (residents or general radiologists). Although the diagnostic accuracy of an experienced specialist may be the same as that of our CAD, our system tends to improve the consistency of this procedure.

2 Materials and methods

In this study, we selected four types of MR images that were considered most informative with regard to the diagnosis of focal liver disease.

2.1 MR imaging of the liver

The basic principle underlying the diagnosis of focal liver lesions with MR imaging is based on the difference in signal intensity between liver lesions and liver parenchyma, internal architecture, and vascularity; these differences are evaluated through the use of T1-weighted images, T2-weighted images, and gadolinium-enhanced images obtained in the hepatic arterial phase and the equilibrium phase that occur at approximately 25 s and 3 min, respectively, after the initiation of an intravenous bolus injection of gadolinium chelate solution [14].

Precontrast T1-weighted MR images are ordinarily obtained using a spin-echo or gradient-recalled-echo sequence. In our experiment, the repetition time/echo time was set at 316 ms/11 ms, as shown in Fig. 1a. Further, FSE T2-weighted imaging, which has been shown to play a key role in the characterization of liver lesions [15–19], is performed using an FSE sequence. The signal intensities of metastases for T1- and T2-weighted images are variable, but are usually prolonged. T2-weighted imaging is reported to be very effective in enabling radiologists to differentiate between cavernous hemangiomas and metastases [20–25]. In our experiment, the effective TR/effective TE of FSE T2-weighted images was set at 4615 ms/80 ms, as shown in Fig. 1b.

HCCs often appear less hyperintense and less conspicuous in T2-weighted images, but are often readily detected and characterized on enhanced MR images.

Through the use of gadolinium-enhanced dynamic MR imaging of the liver, three different phases of images—hepatic arterial, portal venous, and equilibrium phases—can be obtained for the effective differentiation of focal liver lesions. In these images, hepatic cysts are not enhanced throughout the three phases, cavernous hemangiomas are enhanced as intensely as the vessels in each phase, and HCCs are often rapidly enhanced in the hepatic arterial phase and show a washout in the equilibrium phase. In addition, dysplasias in cirrhosis appear hyperintense on unenhanced T1-weighted images, but are never found to be enhanced in gadolinium-enhanced images, and metastases often show no enhancement or ring-like enhancement in hepatic arterial-phase images.

Radiologists diagnose focal liver lesions based on such complex MR imaging findings for different focal liver diseases. Examples of the hepatic arterial and equilibrium-phase images are shown in Fig. 1c and d, respectively. With a 1.5-T superconducting magnet (Signa Horizon; GE Medical Systems, Milwaukee, WI, USA), 320 MR images of 80 patients (four images per patient) who had focal liver lesions were obtained. These cases were diagnosed by two experienced radiologists, and the majority of them were confirmed pathologically from biopsy or surgery. Although

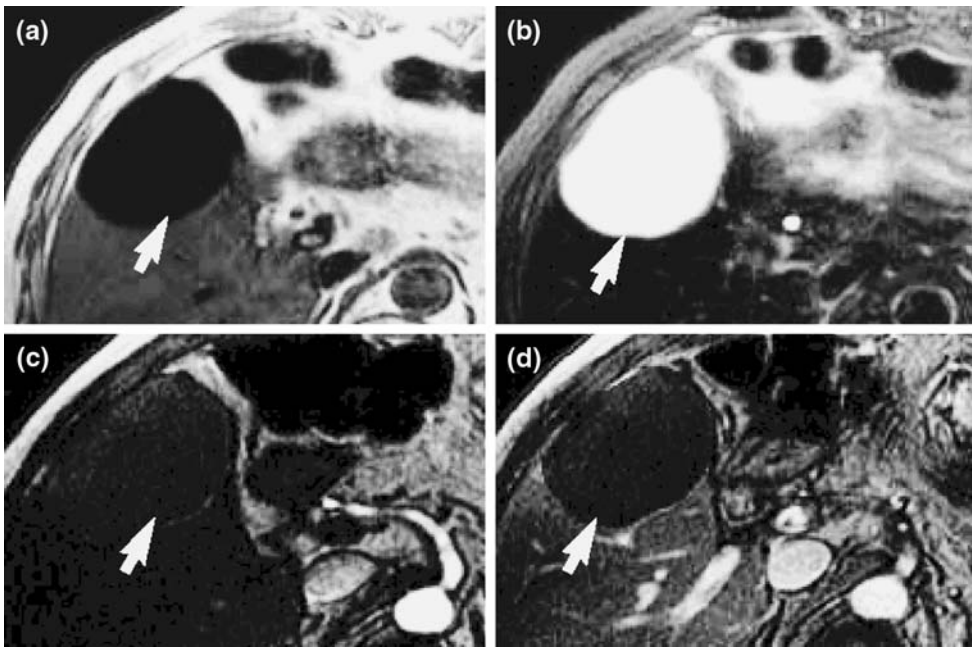

Fig. 1 Four ROIs (*arrows*) of lesions in the same case of a cyst show different intensities and homogeneity. **a** T1-weighted spin-echo image [316/11 (repetition time ms/echo time ms)]. ROI indicates cyst shown as a hyperintense area, which is darker than the liver, with an intensity value of 0.1 assigned by the computer. **b** T2-weighted fast spin-echo image [4615/80 (effective TR/effective TE)]. *Arrow* indicates hyperintense area that is brighter than liver metastasis. Signal intensity and homogeneity were assigned values of 0.9 and 0.9, respectively. **c** Gadolinium-enhanced hepatic arterial-phase gradient-recalled-echo image [150/1.6 (TR/TE)] appears very dark. The signal intensity of this lesion was assigned a value of 0.1. **d** Gadolinium-enhanced equilibrium-phase gradient-recalled-echo [150/1.6 (TR/TE)] image. Signal intensity inside the lesion is very low, with an assigned value of 0.1

it is impossible to diagnose all lesions pathologically, the remaining patients underwent angiography-assisted ultrasonography, CT, or follow-up MR imaging for confirmation of the diagnosis. Our criterion for diagnosing malignancy is rather stringent, with the exception of cases in which the lesion size is very small; such cases were not included in this study.

2.2 Logic classifier

MR imaging provides different types of images, and a diagnosis is made by interpreting the complicated imaging findings. Figure 2 shows a typical flowchart of MR imaging findings observed for focal liver lesions with different pathologies. Based on the fundamental MR imaging characteristics of each pathologic type from the flowchart, establishing a multiple logistic tree is not difficult. For the first scenario for our program that we considered, check box items were included in order to select intensity attributes in four MR images and the homogeneity of T2-weighted images. However, this method includes some subjective parameters: for example, the continual intensity value can be divided into three choices, which may cause deviation from the decision when choosing between low and iso (having the same intensity as the liver tissue), intermediately high and high, homogeneous (low variance), or heterogeneous (high variance), and so on. Such subjective parameters may influence the diagnosis. Moreover, in the diagnosis of more complicated cases, the relationship among these parameters can be much more complicated than that indicated in Fig. 2. The addition of new cases or new types of images requires the reconstruction of the logistic tree. Thus, one solution to these problems is to establish an algorithm that can take in continuous values as inputs and automatically adjust the relationship between the input parameters and outputs. The characteristics of the neural-network paradigm are suitable for these requirements, and such networks have a powerful ability to solve such classified problems efficiently.

2.3 Artificial neural network and its architecture

Artificial neural networks (ANNs), which have been successfully applied in many fields related to medical imaging [26–29], make it easy for less experienced doctors to make a correct diagnosis by inferring new inspections from past experience. We have developed software named "Liver-ANN" [30, 31], based on ANN technology, for the diagnosis of focal liver disease. The network is trained using the well-known back-propagation (BP) algorithm [32]. After establishing the relationship function between the inputs and outputs, we apply the ANN to the doctors'

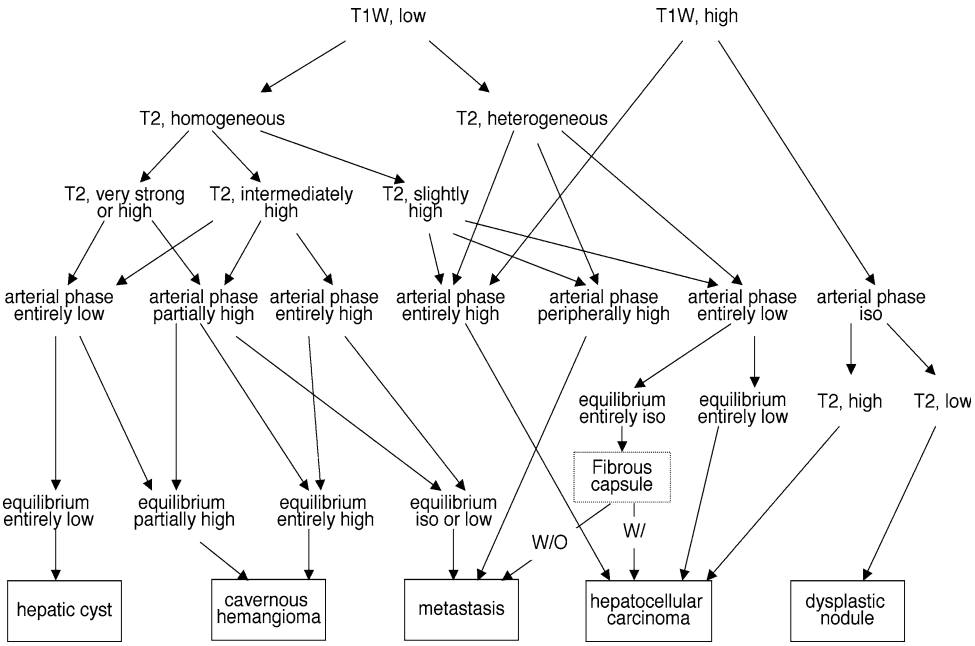

Fig. 2 Diagnostic flowchart for hepatic lesions used in a doctors' routine check. The procedure is based on the intensity and homogeneity of the MRI signal

practical routine inspection to test the generalization ability of the ANN.

Unlike a logistic tree, neural networks are not designed based on explicit data and rules, but on numerous samples. A knowledge-based neural network (KBNN) [33] provides a method of combining the advantages of the above two methods. The ideal approach would be to develop neural network connections in accordance with Fig. 2, and then to train the network by providing samples. However, it is uncertain whether the relationship depicted in Fig. 2 is complete. Some exceptional cases might be present.

Therefore, in this study we developed a fully connected neural network, as shown in Fig. 3, which is a conventional three-layer feed-forward neural network with five input units, eight hidden units, and five output units. The selection of hidden layer units is decided by the complexity of the case data. If the number of units is less than five, the learning procedure of the ANN becomes slow and convergence is difficult, resulting in a failure to differentiate, even for the training dataset. Therefore, we selected eight or more hidden units in our experiment. The network learning rate was set to 0.9, the momentum factor to 0.3, and the number of training iterations was always 1700–2500, with a 100% training accuracy. Similar to the inspection method employed by radiologists, we applied the visual features on the MR image to train the network. The five input units are the homogeneity from T2-weighted MR imaging and the intensities from four MR imagings, namely: T1-weighted MR imaging, T2-weighted MR imaging, dynamic arterial phase, and dynamic equilibrium phase. The outputs are the five categories of hepatic diseases—liver cyst, cavernous hemangioma, dysplasia in cirrhosis, HCC, and metastasis.

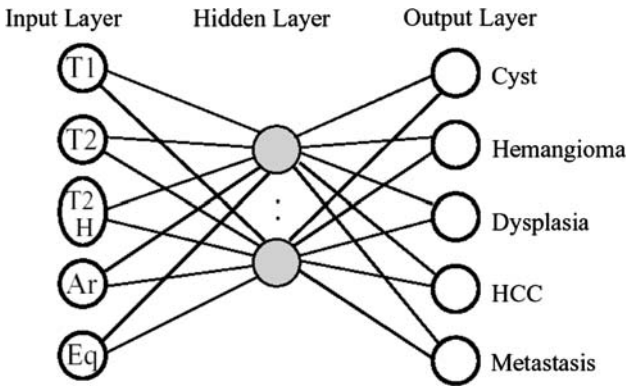

Fig. 3 A multilayer feed-forward network used in LiverANN can automatically find the internal connections between inputs and outputs by learning from samples using a back-propagation algorithm was employed. *T2H* homogeneity of T2-weighted imaging, *Ar* arterial, *Eq* equilibrium, *HCC* hepatocellular carcinoma

2.4 Input selection

Extracting a lesion region from liver parenchyma using a computer algorithm is still a difficult task because the intensities of the four abovementioned MR images are quite different and random, and the intensity of a lesion may appear strong in one image but subtle in another. For a heterogeneous case in particular, varying gray values cause the border of a region of interest (ROI) to be irregular, leading to an incorrect calculation of mean values within the ROI. Furthermore, differences in imaging times make it impossible to propagate a selected ROI of the same size and location from a T1-weighted image to T2-weighted, post-contrast early-phase, and late-phase images.

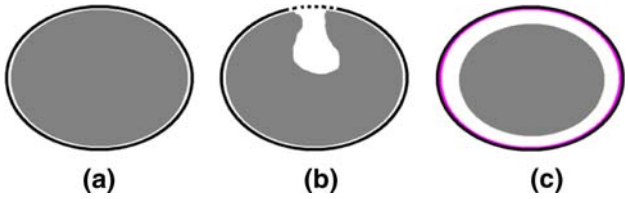

Fig. 4 Guidelines for determining the lesion borders of ROI in **a** a homogeneous case, **b** a heterogeneous case, and **c** an enhanced case

The current version of LiverANN provides a paint toolbox that allows radiologists to delineate ROIs using a mouse. A border is drawn along the lesion edge in the homogeneous case, as shown in Fig. 4a. An estimated drawing (broken line) is interpolated in order to maintain the shape of a lesion in the heterogeneous case, as shown in Fig. 4b. If the lesion is enhanced, the ROI will include the periphery or normal hepatic parenchyma surrounding the lesion, as seen in Fig. 4c. In a hepatic MR case, first, the lesion regions in the T1-weighted, T2-weighted, dynamic arterial phase, and dynamic equilibrium phase images are selected by a specialist, and then the program automatically calculates the average intensity as the intensity in the ROI; the standard deviation value is inversely proportional to the homogeneity.

Because all elements of the training dataset must be scaled appropriately, the four intensities and the T2 homogeneity are normalized into numerical data between 0 and 1 before they are fed into the ANN as inputs. After normalization,

$$g_{\text{in}} = \frac{1}{2^n} g_{\text{ave}}, \tag{3}$$

$$D_{\text{in}} = 1 - \frac{1}{2^{n-1}} D, \tag{4}$$

Here, g_{in} and D_{in} are the average intensity and homogeneity, respectively, in a selected ROI (inputs for the ANN); n is the bit value of $g(x, y)$; g_{ave} is the mean gray level; and D is the standard deviation of the ROI.

Datasets from 1999 to 2001 at the Medical School of Gifu University, Japan, were selected. An experienced radiologist attempted to collect MR images with different image findings in lesions as much as possible in order to train the ANN, and randomly selected cases in order to test the generating ability of the ANN. A total of 50 focal liver lesions, including liver cysts ($n = 10$), cavernous hemangiomas ($n = 10$), dysplasias in cirrhosis ($n = 10$), HCCs ($n = 10$), and metastases ($n = 10$), were used to train the ANN, whereas the remaining 30 cases, which were separated into the five categories of liver diseases (each category contained six cases), were used to test the performance of the ANN. The optimum architecture of the combination of cases was selected through a trial-and-error process during the training and testing procedures of the ANN.

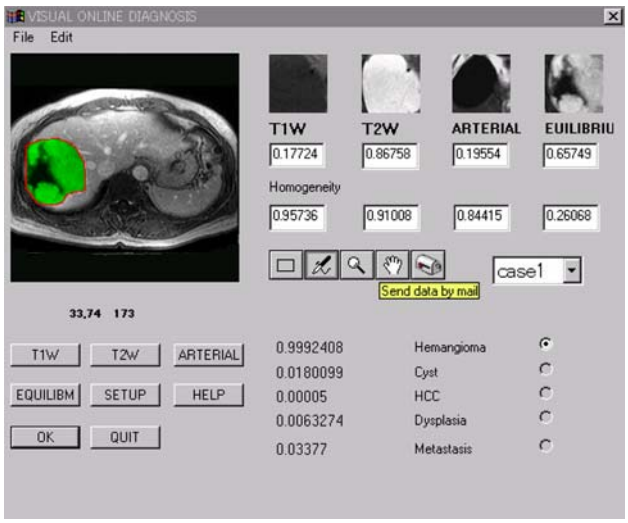

Fig. 5 The graphical user interface of the LiverANN. The main window changes when one of the four MR buttons corresponding to the T1- and T2-weighted, dynamic arterial, and equilibrium-phase images is pressed. The four subimages show the region containing ROIs, as selected from four MR images by a doctor. The intensities and homogeneity of the ROIs are calculated automatically. Outputs of the ANN indicate the likelihood (0–1.0) of each liver disease

2.5 Graphical user interface of LiverANN program

Our software was built using the REALbasic language running on a Macintosh computer; it can run on Mac OS, Windows OS, or Linux. Therefore, users can select the software for their own convenience. As shown in Fig. 5, the graphical user interface comprises several parts—image-selecting buttons, one main display window, and six subwindows (pre-contrast and portal venous phase images are available as well), drawing tool panels, a data-display or text-input box, and a disease result indicator. Using the sendmail function of LiverANN, remotely located radiologists can easily send unknown data to our research laboratory with information on an unexpected type of lesion. This function is expected to be one of the most important resources of retraining data for the ANN. Because the efficiency of the training process is very high, we can use these training datasets as tutorials for educating inexperienced radiologists using images in the LiverANN.

3 Results

The output produced by the LiverANN in the case of the cyst shown in Fig. 1 is indicated in Fig. 6a. Based on this, the cyst item has the highest output value among all five possibilities.

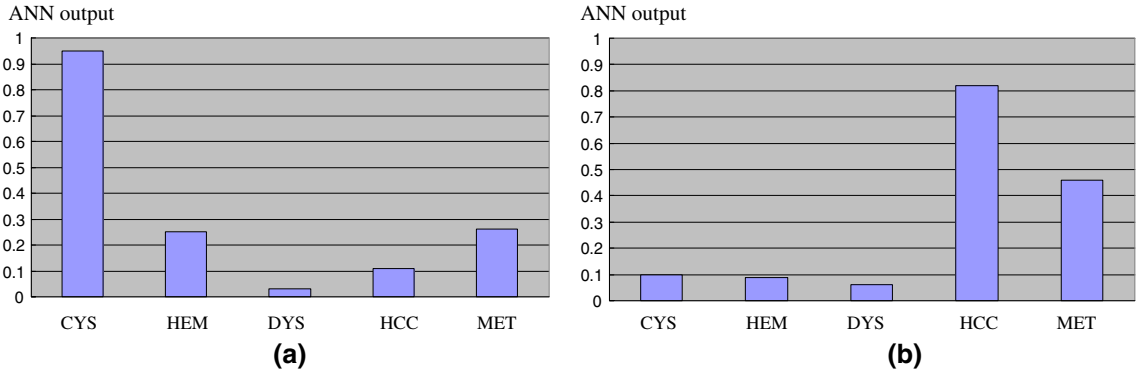

Fig. 6 Classification results from the LiverANN for cases of a cyst (**a**) and hepatocellular carcinoma (**b**). *CYS* cyst, *HEM* hemangioma, *DYS* dysplastic nodule, *HCC* hepatocellular carcinoma, *MET* metastasis

Table 1 Classification results for 30 test cases: two cases judged by a doctor as hepatocellular carcinomas were categorized incorrectly as metastases by the LiverANN

Doctor	LiverANN				
	Liver cyst	Cavernous hemangioma	Dysplasia in cirrhosis	Hepatocellular carcinoma	Metastasis
Liver cyst	6	0	0	0	0
Cavernous hemangioma	0	6	0	0	0
Dysplasia in cirrhosis	0	0	6	0	0
Hepatocellular carcinoma	0	0	0	4	2
Metastasis	0	0	0	0	6

The initial results showed that the LiverANN could classify 50 cases of the training dataset and 30 test cases into the five types of focal liver lesions; the training accuracy in the former set was 100%, whereas the testing accuracy in the latter set was optimally 93.3% (28/30). Figure 6a is a correctly classified example of a liver cyst, and Fig. 6b is an incorrectly characterized HCC. Table 1 shows the difference between the results obtained for the 30 test cases when they were evaluated by an experienced radiologist and the results obtained when the LiverANN was employed. The LiverANN wrongly categorized two HCCs as metastases.

4 Discussion

Focal liver lesions can be accurately detected and characterized with MR imaging. The misdiagnosis made by the LiverANN may have occurred because some HCCs are mildly hyperintense in T2-weighted images, moderately hypervascular in the hepatic arterial phase, and hypointense in the equilibrium phase. Hypervascular metastases such as renal cell carcinoma or carcinoid tumor have brisk arterial enhancement and may be indistinguishable from HCC. The broad spectrum of enhancement patterns or the morphology of HCC makes it difficult to characterize this type of tumor using the CAD algorithm, and some overlap in imaging features is observed between HCC and metastasis in daily clinical practice. Information on other features, such as the presence of fibrous encompassing capsules or cirrhotic changes around the focal liver lesions, an elevated serum alpha-fetoprotein (AFP) level, or a history of extrahepatic primary cancer, is critical in differentiating between HCC and metastasis, and such supplementary information other than the signal intensity and the homogeneity of lesions is very helpful to radiologists attempting to correctly interpret MR images.

It is difficult to collect a sufficient number of clinical cases at one time or in one place to train the ANN. Our LiverANN program provides a data-transmitting function for collecting ANN-training data through a network or via the Internet. Figure 7 illustrates a data collection system procedure. The ANN is first trained with a basic dataset on a Sun workstation in the X Window C language. After the weights between neurons have been decided, a version of the LiverANN can be developed under the REALbasic language and then sent to a hospital to be employed by the doctors for their routine inspections. If the LiverANN cannot correctly identify a new case, these data will be used to retrain the ANN via the sendmail function of the LiverANN from hospitals. On the other hand, if the case is correctly identified, it will be omitted because the ANN already has the ability to deal with such a case. A new version of LiverANN that has been trained with a new

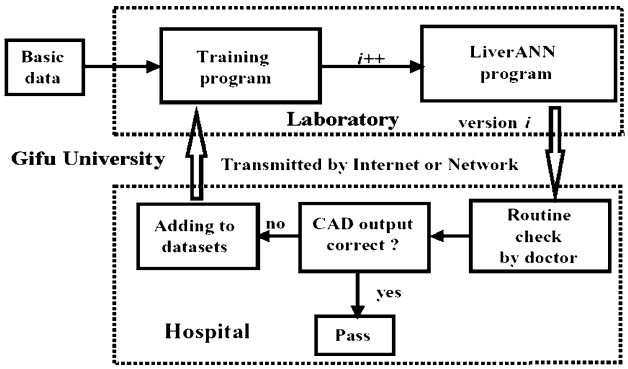

Fig. 7 Data collection system for ensuring that the collection of retraining data is performed between our research laboratory and the university hospital via a network or the Internet

dataset will be sent out to hospitals so as to obtain more data on which the LiverANN has not been trained. This loop will be continued until a satisfactory clinical result is obtained.

Furthermore, including shape or enhancement characteristics in the imaging feature descriptors may also improve the interpreting ability of the LiverANN in some difficult cases. It is well established that hemangiomas are identified by their characteristic peripheral contrast enhancement rather than by the magnitude of their signal intensity. In the absence of this unique geographic enhancement pattern, it would be extremely difficult to differentiate an HCC from a metastasis. In addition, the enhancement pattern of metastases is highly dependent on the type and vascularity of the primary cancer. A hypervascular metastasis is often indistinguishable from HCC based on the imaging features alone. The presence of cirrhosis and a patient's clinical and laboratory data are helpful in making the diagnosis. The integration of such additional information into the LiverANN will be the next step in this study.

We did not include portal-venous-phase images among the input data used in this study, because hepatic arterial and equilibrium-phase images often provide sufficient information on lesion vascularity, and that input data should be simplified. However, we may need to include information on portal-venous-phase images to raise the diagnostic accuracy of the LiverANN, because radiologists usually consider the three phases of gadolinium-enhanced images as well as the T1- and T2-weighted images in a clinical setting.

In this study, although the quantitative ROI data for focal liver lesions selected manually by radiologists showed no significant interobserver variability, in order to rectify possible inconsistencies in diagnosis among radiologists, we plan to identify the ROI by means of an automated image feature-extraction technique in the next step.

5 Conclusion

Our initial trial aimed at characterizing focal liver diseases using the LiverANN program demonstrated the ability of the program to fuse the complex imaging findings with different imaging sequences obtained during individual MR imaging of the liver. By adding different types of input parameters and training data, the program may be able to analyze more complicated imaging findings, thereby providing radiologists with a more useful second opinion. This program is also useful to radiologists for educational purposes during practical diagnostic procedures.

Acknowledgments This research was supported in part by the National Natural Science Foundations of China (No. 60863014 and 60762001); in part by the Program to Sponsor Teams for Innovation in the Construction of Talent Highlands in Guangxi Institutions of Higher Learning; in part by the National Creative Plan for Undergraduate Students of Guangxi University (No. 200707 and X071036); in part by a research foundation project of the Guangxi Ministry of Education (No. 200810MS048); and in part by a research grant from the Collaborative Centre for Academy/Industry/Government of Gifu University, the Ministry of Health, Labor, and Welfare under a Grant-In-Aid for Cancer Research, and the Ministry of Education, Culture, Sports, Science and Technology under a Grant-In-Aid for Scientific Research by the Japanese Government.

References

1. Landis S, Murray T, Bolden S. Cancer statistics. CA Cancer J Clin. 1999;49:8–31.
2. Matsui O, Kadoya M, Kameyama T. Adenomatous hyperplastic nodules in the cirrhotic liver: differentiation from hepatocellular carcinoma with MR imaging. Radiology. 1989;173:123–6.
3. Garra B, Insana M, Shawker T, Russell M. Quantitative estimation of liver attenuation and echogenicity: normal state versus diffuse liver disease. Radiology. 1994;14:1099–108.
4. Hartman P, Oosterveld B, Thijssen J, Rosenbusch G. Detection and differentiation of diffuse liver disease by quantitative echography: a retrospective assessment. Invest Radiol. 1993;28:1–6.
5. Gosnik B, Lemon S, Scheible W, Leupold G. Accuracy of ultrasonography in diagnosis of hepatocellular disease. Am J Roentgenol. 1979;133:19–23.
6. Foster K, Dewbury K, Griffith A, Wright R. The accuracy of ultrasound in the detection of fatty infiltration of the liver. Br J Radiol. 1980;53:440–2.
7. Ogawa K, Fukushima M, Kubota K, Hisa N. Computer-aided diagnosis system for diffuse liver diseases with ultrasonography by neural network. IEEE Trans Nucl Sci. 1998;45:3069–74.
8. Wang Y, Itph K, Sum S. Study on tissue characterization by texture analysis with co-occurrence matrix method using ultrasonography and CT imaging. J Med Ultrason. 2002;29:211–23.
9. Bae K, Giger M, Chen C. Automatic segmentation of liver structure in CT images. Med Phys. 1993;20:71–8.
10. Selle D, Preim B, Schenk A. Analysis of vasculature for liver surgical planning. IEEE Trans Med Imaging. 2002;21:1344–57.
11. Tombropoulos R, Shiffman S, Davidson C. A decision aid for diagnosis of liver lesions on MRI. Proc Annu Symp Comput Appl Med Care. 1993;439–43.

12. Maclin PS, Dempsey J. How to improve a neural network for early detection of hepatic cancer. Cancer Lett. 1994;77:95–101.
13. Genevieve L, Andrea P, Williamand W, Peter F, Wolfgang S, Sanjay S. Addition of gadolinium chelates to heavily T2-weighted MR imaging: limited role in differentiating hepatic hemangiomas from metastases. Am J Roentgenol. 2000;174:477–85.
14. Honda H, Matsuura Y, Onitsuka H. Differential diagnosis of hepatic tumors (hepatoma, hemangioma, and metastasis) with CT: value of two-phase incremental imaging. Am J Roentgenol. 1992;159:735–40.
15. Whitney W, Herfkens R, Jeffrey R, McDonnell C, Li K, Dalsem W, et al. Dynamic breath-hold multiplanar spoiled gradient-recalled MR imaging with gadolinium enhancement for differentiating hepatic hemangiomas from malignancies at 1.5 T. Radiology. 1993;189:863–70.
16. Hamm B, Fischer E, Taupitz M. Differentiation of hepatic hemangiomas from metastases by dynamic contrast-enhanced MR imaging. J Comput Assist Tomogr. 1990;14:205–16.
17. Hamm B, Thoeni RF, Gould R, Bernardino M, Luning M, Saini S, et al. Focal liver lesions: characterization with nonenhanced and dynamic contrast material enhanced MR imaging. Radiology. 1994;190:417–23.
18. Semelka R, Brown E, Ascher S, Patt R, Bagley A, Li W, et al. Hepatic hemangiomas: a multi-institutional study of appearance on T2-weighted and serial gadolinium-enhanced images. Radiology. 1994;192:401–6.
19. Semelka R, Shoenut J, Kroeker M, Greenberg H, Simm F, Minuk G, et al. Focal liver disease: comparison of dynamic contrast-enhanced CT and T2-weighted fat suppressed, FLASH, and dynamic gadolinium enhanced MR imaging at 1.5 T. Radiology. 1992;184:687–94.
20. Mergo P, Ros PR. Benign lesions of the liver. Radiol Clin North Am. 1998;36:319–31.
12. Lombardo DM, Baker ME, Spritzer CE, Blinder R, Meyers W, Herfkens RJ. Hepatic hemangiomas vs metastases: MR differentiation at 1.5 T. Am J Roentgenol. 1990;155:55–9.
22. Itoh K, Saini S, Hahn P, Imam N, Ferrucci J. Differentiation between small hepatic hemangiomas and metastases on MR images: importance of size-specific quantitative criteria. Am J Roentgenol. 1990;155:61–6.
23. Li K, Glazer G, Quint L, Francis I, Aisen A, Ensminger W, et al. Distinction of hepatic cavernous hemangioma from hepatic metastases with MR imaging. Radiology. 1988;169:409–15.
24. Brown J, Lee M, Lee J, Lom K, Malchow S. Focal hepatic lesions: differentiation with MR imaging at 0.5 T. Radiology. 1991;179:675–9.
25. Mirowitz S, Lee J, Heiken J. Cavernous hemangioma of the liver: assessment of MR tissue specificity with a simplified T2 index. J Comput Assist Tomogr. 1990;14:223–8.
26. Asada N, Doi K, MacMahon H, Montner S, Giger ML, Abe C, et al. Potential usefulness of an artificial neural network for differential diagnosis of interstitial lung disease: pilot study. Radiology. 1990;177:857–60.
27. Fujita H, Katafuchi T, Uehara T, Nishimura T. Application of artificial neural network to computer-aided diagnosis of coronary artery disease in myocardial SPECT bull's-eye images. J Nucl Med. 1992;33:272–6.
28. Zhang W, Doi K, Giger M, Nishikawa R, Schmidt R. An improved shift-invariant artificial neural network for computerized detection of clustered microcalcifications in digital mammograms. Med Phys. 1996;23:595–601.
29. Seki K, Fujita H, Hirako K, Hara T, Ando T. Detection of microcalcifications on mammograms using neural networks. Med Imag Tech. 1997;15:639–51.
30. Kako N, Zhang X, Kanematsu M. Study of computer-aided diagnosis on MR imaging. Radiology. 2002;255(P):749. (abstract).
31. Kako N, Zhang X, Li W. Artificial neural network method for differentiation of focal liver disease in MR imaging. Radiology. 2002;255(P):646.
32. Rumelhart D, McClellend J. Learning representations by back-propagating errors. Nature. 1986;323:533–6.
33. Towell G. Knowledge-based artificial neural networks. Artif Intell. 1994;70:119–65.